Visualization of the structure of vortex breakdown in free swirling jet flow

Maarten Vanierschot[1,*], Mustafa Percin[2], Bas W. van Oudheusden[2]
1: Dept. of Mechanical Engineering, KU Leuven, Belgium
2: Dept. of Aerospace Engineering, Delft University of Technology, the Netherlands
* Correspondent author: maarten.vanierschot@kuleuven.be

Keywords: Swirling annular jet, Tomographic PIV, Pressure reconstruction, Vortex breakdown

ABSTRACT

In this paper we investigate the three dimensional flow structures in a free annular swirling jet flow undergoing vortex breakdown. The flow field is analyzed by means of time-resolved Tomographic Particle Image Velocimetry measurements. Both time-averaged and instantaneous flow structures are discussed, including a detailed analysis of the first and second order statistical moments. A Reynolds decomposition of the flow field shows that the time averaged flow is axisymmetric with regions of high anisotropic Reynolds stresses. Two recirculation zones exist with regions of very intensive mixing around them. Despite the axisymmetric nature of the time-averaged flow, a non-axisymmetric structure of the instantaneous flow is revealed, including a central vortex core which breaks up into a double helix. The winding sense of this double helix is opposite to the swirl direction and it is wrapped around the vortex breakdown bubble. The double helix precesses around the central axis of the flow with a precessing frequency corresponding to a Strouhal number of 0.13. To the authors' knowledge, this structure of vortex breakdown has not been previously reported in the literature to occur for turbulent jet flow and it suggests that the well-known Precessing Vortex Core (PVC) found in swirling jets corresponds to the helical mode of vortex breakdown.

1. Introduction

Annular jet flows are of practical interest in view of their occurrence in many industrial applications in the context of bluff-body combustors (Gupta et al. 1986). They feature different complex flow characteristics despite their simple geometry: a central recirculation zone (CRZ) as a result of flow separation behind the centerbody and an outer (between the jet and the environment) and inner (between the jet and the central recirculation region) shear layer, which are both characterized by strong anisotropic turbulence (Vanierschot et al. 2014). The complexity of the flow is further enhanced when introducing swirl which leads to the formation of large zones of recirculation and large scale instabilities at certain swirl numbers, such as vortex breakdown or a precessing vortex core (PVC) (Vanierschot and Van den Bulck 2008, Lucca-Negro and O'Doherty 2001). These large coherent structures have been well studied for round jets. However, for the case of annular jet flows, much remains to be resolved, especially regarding the interaction between the instabilities and the CRZ. The specific aim of the current study is therefore to investigate the spatial

and temporal characteristics of these three-dimensional flow fields, employing time-resolved tomographic particle image velocimetry (Tomo-PIV) measurements (Elsinga et al. 2006, Scarano 2012). The time averaged flow field is found to be axisymmetric with a central recirculation bubble. However, looking at the transient features of the flow, a central vortex core is observed which precesses around the central axis and breaks up into a double helix when the flow becomes critical. This double helix mode of vortex breakdown is very rare and all recent studies in literature only report it in the wake of an axisymmetric bubble (Ruith et al. 2003). The present study is the first one to show that the vortex core already breaks up upstream of the vortex breakdown bubble and that it precesses around the central axis. This suggests that the well-known precessing vortex core found in swirling flows is actually the spiral mode of vortex breakdown. To the authors' knowledge, this study is the first one to make the connection between these two flow features found in swirling jets.

2. Experimental Setup & Processing Methods

2.1. Experimental setup

The experiments were conducted in a water tank facility at the Aerodynamic Laboratories of Delft University of Technology. An annular jet orifice with an inner diameter D_i = 18 mm and an outer diameter D_o = 27 mm was installed at the bottom wall of the octagonal water tank (600 mm of diameter and 800 mm of height), which is made of Plexiglass to enable full optical access for illumination and tomographic imaging (Percin and van Oudheusden 2015). The symmetry axis of the jet is aligned with the (vertical) y-axis in the measurement coordinate system with the origin located at the exit of the inner tube. The experiments were performed at a Reynolds number of 8,500 based on the hydraulic diameter of the annular jet (D_h = 9 mm) and the mean axial velocity of the jet (U_o = 0.94 m/s). The flow in the system was driven by a pump that was submerged in a reservoir containing water mixed with seeding particles. The swirl was generated by means of a moveable block swirl generator, which consists of 12 guide vanes that can be adjusted to change the swirl strength. In this study, the swirl number based on the ratio of tangential and axial momentum times outer radius is 0.4.

2.1. Tomographic particle image velocimetry

Neutrally buoyant polyamide spherical particles of 56 μm mean diameter were employed as tracer particles at a concentration of 0.65 particles/mm^3. The flow was illuminated by a double-pulse Nd:YLF laser (Quantronix Darwin Duo, 2 × 25 mJ/pulse at 1 kHz) at a wavelength of 527 nm. The

light scattered by the particles was recorded by a tomographic system composed of four LaVision HighSpeedStar 6 CMOS cameras (1024 × 1024 pixels, 5400 frames/s, pixel pitch of 20 μm). Each camera was equipped with a Nikon 105 mm focal objective with a numerical aperture $f_\# = 32$ to allow focused imaging of the illuminated particles. The measurements were performed in a cylindrical volume with a diameter of $3.6D_n$ and a height of $5.3D_n$ at a digital resolution of 21.6 pixels/mm. The choice of a cylindrical measurement volume eliminated the need for a lens-tilt mechanism to comply with the Scheimpflug condition. Moreover, the cylindrical volume brings about a more favorable condition for the accurate reconstruction since the particle image density does not vary with the viewing angle along the azimuth and decreases when moving toward the periphery of the jet. The average particle image density is approximately 0.045 particles per pixel (ppp). The images were captured with two recording modes: (1) a double-frame mode at a low recording frequency of 50 Hz to allow a converged statistical analysis by using statistical independent samples and capturing the flow for a longer period of time; (2) a single-frame mode at a high recording frequency of 2.5 kHz to enable the visualization of time-series phenomena. In the former case, a total of 2414 images were captured over a duration of 48.3 s, whereas for the latter the measurement duration was limited to approximately 2.2 s.

Image pre-processing, volume calibration, self-calibration, reconstruction and three-dimensional cross-correlation-based interrogation were performed in LaVision DaVis 8.1.6. The measurement volume was calibrated by scanning a calibration target through the measurement volume. The initial calibration was refined by means of the volume self-calibration technique, resulting in a misalignment less than 0.05 pixels. The raw images were pre-processed with background intensity removal and particle intensity normalization. The particle images were then interrogated using windows of final size 48 × 48 × 48 voxels with an overlap factor of 75 %, resulting in a vector spacing of 0.56 mm in each direction.

2.3. Calculation of the mean pressure field

The three-dimensional velocity fields obtained by means of the tomo-PIV measurements are used for the calculation of the time-averaged pressure field of the annular swirling jet flow. This is achieved by means of Reynolds averaging of the momentum equation (as indicated by the overbar) which allows the mean pressure gradient to be calculated as follows (van Oudheusden 2013):

$$\nabla\bar{p} = -\rho(\overline{\boldsymbol{U}}\cdot\nabla)\overline{\boldsymbol{U}} - \rho\nabla\cdot(\overline{\boldsymbol{uu}}) + \mu\nabla^2\overline{\boldsymbol{U}} \qquad (1)$$

where $\overline{\boldsymbol{U}}$ stands for the time averaged velocity and $\boldsymbol{u}$ for the fluctuating component of the velocity. In this approach, the Reynolds stress terms are to be included in the momentum equation, whereas the time-derivative term is no longer required in the calculation of the pressure gradients. These terms are acquired from the ensemble of 2414 statistically-independent individual velocity fields. Then, for the calculation of the time-averaged pressure field the corresponding Poisson problem is solved for the complete flow field by assigning Dirichlet boundary conditions at the lateral surfaces and Neumann boundary conditions at the upper and lower surfaces of the cylindrical measurement domain.

3. Results

3.1 Accuracy of PIV measurements

In the analysis of flow fields obtained with PIV, two kind of errors are introduced in the calculation of flow field variables. The first error is the convergence error and is a result of the calculation of statistical properties based upon a finite number of samples. Next to the sampling error, a second error arises from the spatial resolution of the PIV measurements. If the spatial resolution of the measurements is the interrogation window size Δ , the maximum wavenumber in the turbulent spectrum that can be measured is $k_{max} = \pi/\Delta$ (Willert and Gharib 1991). Due to low pass filtering in the vector processing, the measured second order statistics are lower compared to the real ones if the size of the interrogation window is too large. In the following, both errors are quantified and it is shown that the results in section 3.2 are accurate enough to serve as a database for the validation of numerical codes.

For the statistical analysis of the flow, N = 2414 statistical independent samples are taken to calculate the first and second order moments of the flow. The convergence error of these moments for velocity component U_i and fluctuating component u_i can be calculated as

$$\delta_{\langle U_i \rangle} = \frac{Z_{\alpha/2}}{\sqrt{N}} \frac{\sqrt{\langle u_i u_i \rangle}}{\langle U_i \rangle}, \quad \delta_{\langle u_i u_i \rangle} = \frac{Z_{\alpha/2}}{\sqrt{2N}} \quad \text{and} \quad \delta_{\langle u_i u_j \rangle} = \frac{Z_{\alpha/2}}{\sqrt{N}} \; (i \neq j), \quad (2)$$

where $Z_{\alpha/2}$ = 1.96 in a 95% confidence interval. This gives an average error of 1.2% for the mean quantities and 3% for the normal and 4% for the shear stress components.

To estimate the error introduced by the finite interrogation window size, the procedure of Alekseenko et al. (2007) is followed. This procedure calculates the Kolmogorov and integral length scales of the flow and provides estimates of the error on the second order statistic based on the

ratio between the window size and these length scales. First, the uncorrected turbulent dissipation rate ε is calculated from the measurements as

$$\varepsilon_{meas} = \nu \langle 2\left(\frac{\partial u_x}{\partial x}\right)^2 + 2\left(\frac{\partial u_y}{\partial y}\right)^2 + 2\left(\frac{\partial u_z}{\partial z}\right)^2 + \left(\frac{\partial u_x}{\partial z} + \frac{\partial u_z}{\partial x}\right)^2 + \left(\frac{\partial u_y}{\partial x} + \frac{\partial u_x}{\partial y}\right)^2 + \left(\frac{\partial u_z}{\partial y} + \frac{\partial u_y}{\partial z}\right)^2 \rangle \qquad (3)$$

This dissipation rate serves as an input for the calculation of the Kolmogorov length scale as $\eta = (\nu^3 f_\varepsilon/\varepsilon_{meas})^{1/4}$, where f_ε is taken to be one at the start of the procedure. From this length scale, the correction factor f_ε can be updated as a function of the ratio Δ/η. With this new correction factor, the Kolmogorov length scale is recalculated and the procedure is repeated until convergence is obtained. For the measurements in this study, the results are summarized in Table 1. The integral length scale L of the flow can be estimated as $L = \left(\frac{u_x'^2+u_y'^2+u_z'^2}{3}\right)^{3/2}/\varepsilon$. Based on the study of Alekseenko et al. (2007), the error for the second order statistics is maximal around 8% and the interrogation size Δ is within the inertial subrange of the turbulent spectrum.

Table 1: Maximum dissipation rate (ε) and Kolmogorov (η) and integral length scale (L) of the flow

Δ [mm]	η × 10² [mm]	ε [m²/s]	L [mm]	Δ / η	Δ / L
1.12	2.4	3.13	2.7	46	0.42

3.2 Time-averaged flow quantities

The analysis of the time averaged flow fields applies a Reynolds decomposition, which divides the velocity vector into mean and fluctuating components. Figure 1 displays the spatial distribution of the mean velocity components $\langle U_x \rangle$, $\langle U_y \rangle$ and $\langle U_Z \rangle$ which in the context of swirling flows represent the radial, axial and azimuthal velocity. All quantities are scaled with respect to the mean axial jet velocity, $U_\circ$. The flow field is axisymmetric and hence a planar representation is sufficient to document the flow structure. As shown in Figure 1a, the axial velocity distribution reveals two large regions of backflow, i.e. negative $\langle U_y \rangle$. The first region is the CRZ directly behind the central body. In case of non-swirling flow, this recirculation zone is closed at a stagnation point in the flow downstream (Vanierschot and Van den Bulck 2008). However swirl induces a radial pressure gradient to balance the centrifugal forces,

$$\frac{\partial p}{\partial r} = \rho \frac{W^2}{r} \qquad (4)$$

where W is the azimuthal velocity in cylindrical coordinates and r is the radial distance from the center of the jet. This swirl-induced pressure gradient opens the CRZ and transforms it into a toroidal vortex, as also found in the study by Vanierschot and Van den Bulck (2008). Fluid is drawn from the sides of the torus to the central axis (Figure 1b) and the axial velocity is positive along this central axis. Due to the conservation of angular momentum, the fluid moving inward from the sides of the torus increases in tangential velocity near the central axis as shown in Figure 1c. The increased tangential velocity makes the flow critical and leads to the second recirculation zone, called vortex breakdown (Lucca-Negro and O'Doherty 2001). Based on the time averaged axial velocity field in Figure 1a, vortex breakdown occurs at $y/D_o \approx 0.8$.

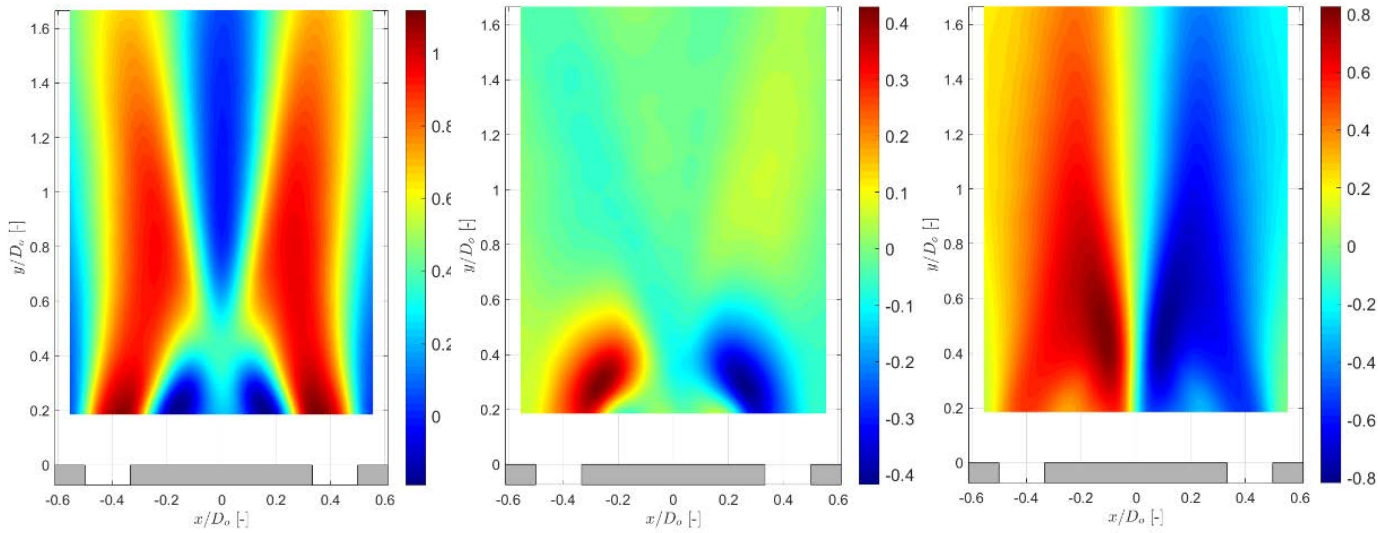

(a) $\langle U_y \rangle / U_o$ (b) $\langle U_x \rangle / U_o$ (c) $\langle U_z \rangle / U_o$

Fig. 1. Mean values of the axial, radial and tangential velocity components.

The second order statistics of the flow field are shown in Figure 2, which reveals that the Reynolds stresses in the flow field are highly anisotropic. Particularly near the CRZ and vortex breakdown bubble, regions of intense mixing occur. Especially the normal stresses in the shear layer between the vortex breakdown bubble and the jet are high and even larger than the stresses in the outer shear layer between jet and environment. This feature of vortex breakdown, namely the intense mixing, is very favorable for combustion applications (Gupta et al. 1986).

The mean pressure field (Fig. 3) reveals the existence of a low-pressure region along the central axis of the jet. This large region originates from the balance between the radial pressure gradient

and the centrifugal forces, as also expressed by Eq. 4. The latter are associated with the large azimuthal velocities occurring particularly downstream of the CRZ (Vanierschot and Van den Bulck, 2008), which can be deduced from the z-component of the velocity as shown in Fig. 1c. The azimuthal velocity decreases in the streamwise direction resulting in an increase of pressure along the jet axis. This positive pressure gradient in the axial direction leads to the vortex breakdown (Lucca-Negro and O'Doherty 2001).

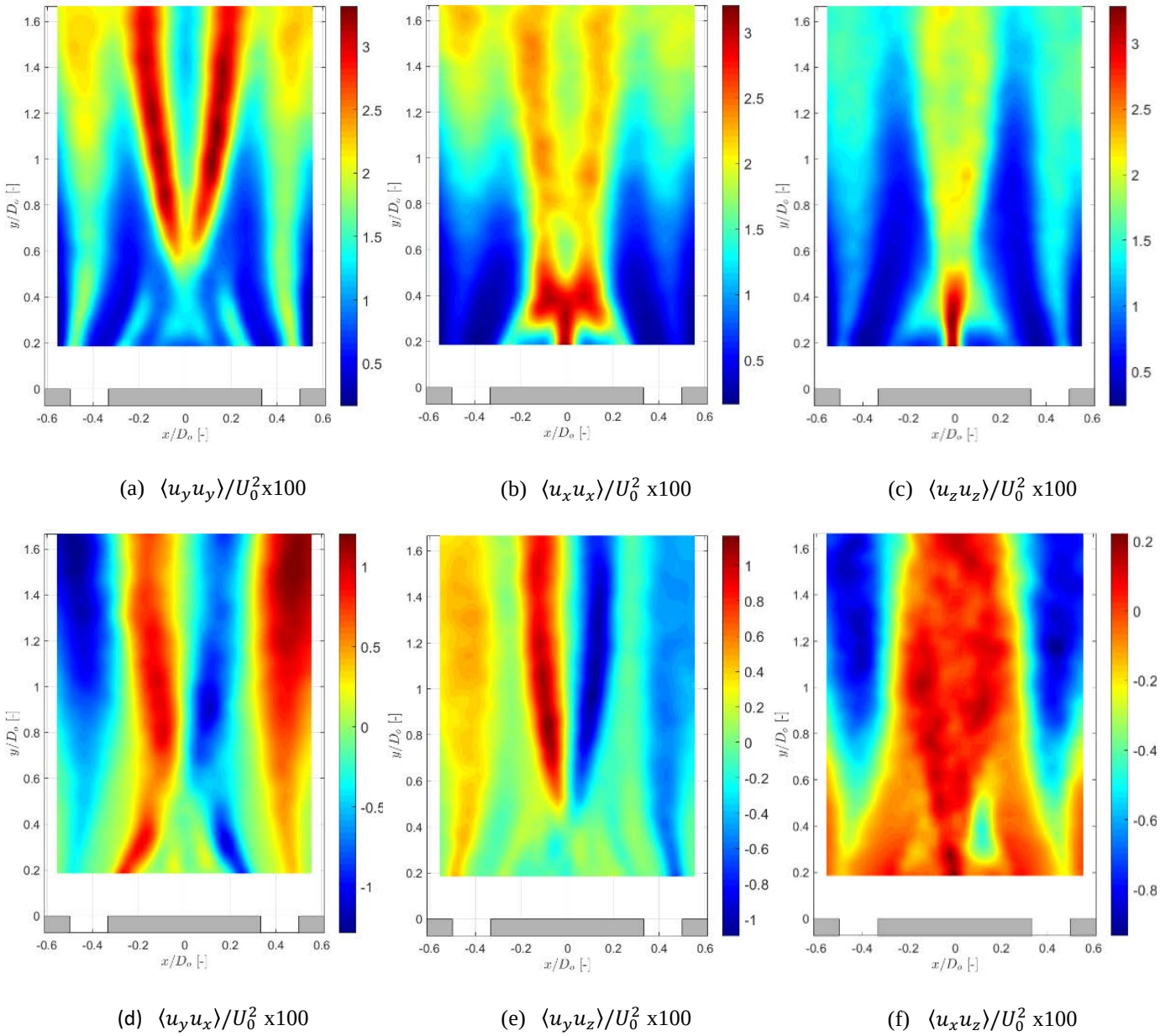

(a) $\langle u_y u_y \rangle / U_0^2$x100 (b) $\langle u_x u_x \rangle / U_0^2$ x100 (c) $\langle u_z u_z \rangle / U_0^2$ x100

(d) $\langle u_y u_x \rangle / U_0^2$ x100 (e) $\langle u_y u_z \rangle / U_0^2$ x100 (f) $\langle u_x u_z \rangle / U_0^2$ x100

Fig. 2. Second order statistics of the flow.

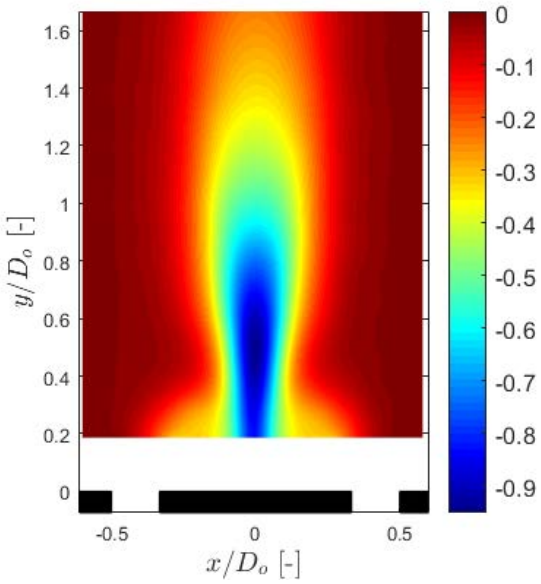

Fig. 3. Normalized mean static pressure field $P/\rho U_0^2$ of the annular swirling jet

3.3 Instantaneous flow structures

In swirling flow, it is well known that large scale vortical structures occur (Lucca-Negro and O'Doherty 2001, Syred 2006). Numerous techniques exist to identify these vortices and in this paper the Q-criterion is applied for this purpose (Jeong and Hussain 1995). This criterion identifies vortices as isosurfaces of positive Q. The instantaneous vortical structures of the jet are shown in Figure 4, which shows isosurfaces of $Q = 1.8.10^3\ 1/s^2$. The black isosurfaces in the figure correspond to contours of zero axial velocity, thus indicating the outer contours of the backflow regions. The left figure (4a) shows the vortical structures as obtained from the raw PIV data. In the flow field, different structures appear associated with both turbulence or large scale coherent structures. The vortices associated to turbulence in the flow can be removed by the Eulerian Time Filtering (ETF) technique as described by Vanierschot et al. (2009) and the results are shown in Figure 4b. Two distinct large scale vortical structures can be observed. The first one is the CRZ, which corresponds to the ring-shaped vortex near the centerbody. The second flow structure is the vortex core along the central axis of the jet.

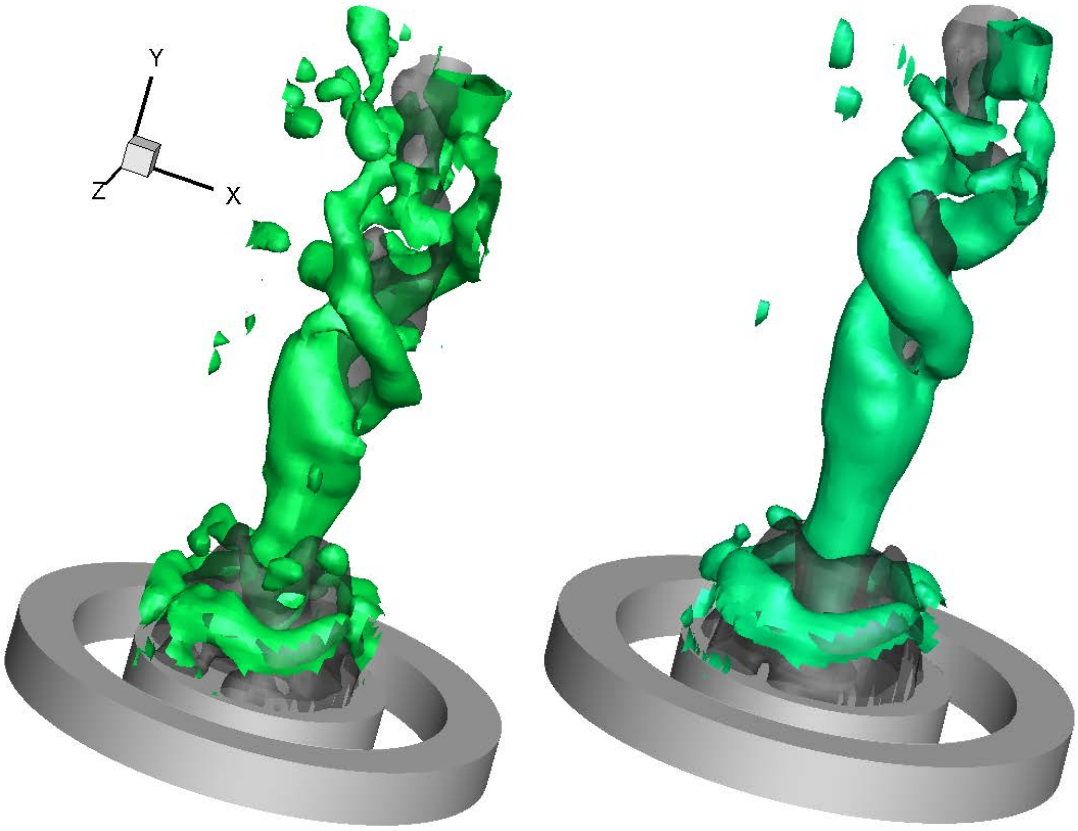

(a) Instantaneous flow structures (b) ETF filtered flow structures

Fig. 4 Vortical structures in the jet.

This vortex core is seen to break up into a double helix shape downstream, which corresponds to the spiral mode of vortex breakdown. The double helix structure is wrapped around the central recirculation zone and it is winding in the opposite direction of the swirl, as has been frequently observed in other studies (Lucca-Negro and O'Doherty 2001). The double helix mode of vortex breakdown is very rare and not many authors have showed it in their experiments. To the author's knowledge, this double helix breakdown has only been reported in laminar flows, so this study would be the first one to identify it for turbulent jet flow.

Temporal analysis of the vortical structures shows that the double helix precesses around the central axis. This feature is well known in literature and is called the precessing vortex core or PVC (Syred 2006). In the jet flow in this study, the precessing frequency is identified by analyzing the PSD at fixed points in the flow field. Figure 5 shows the PSD of the velocity components in two points at $y/D_\circ = 0.4$ and 0.8 on the central axis. A clear peak in the spectra is found at a Strouhal

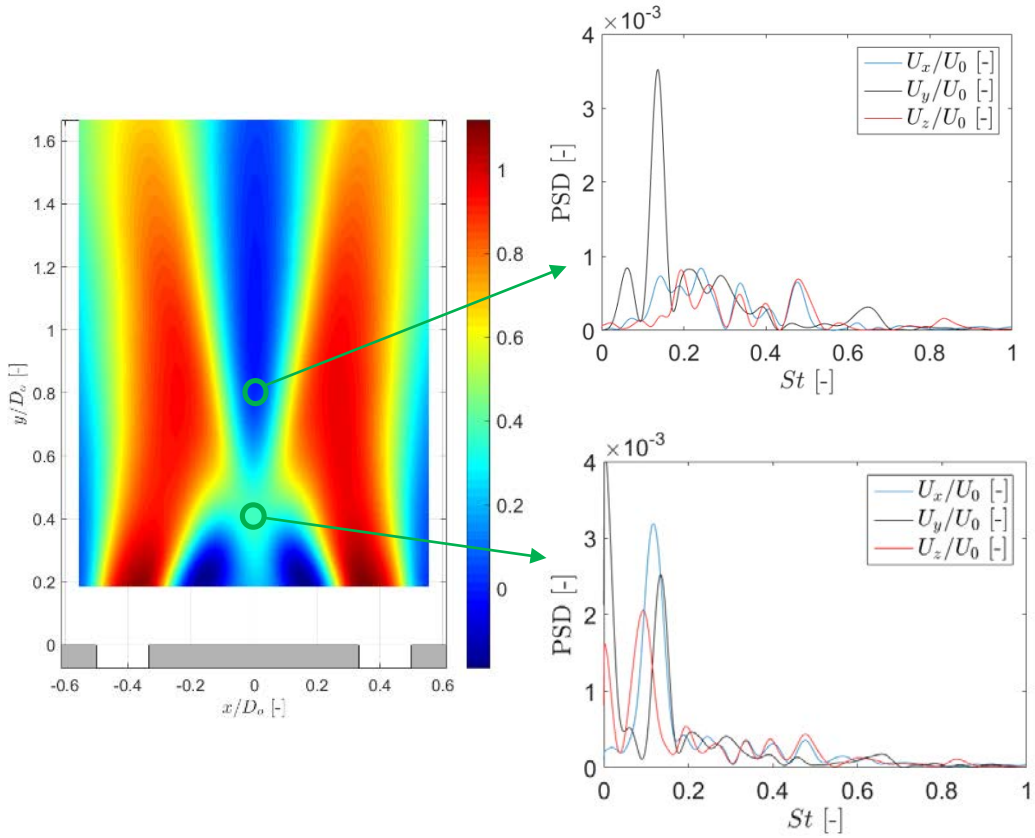

(a) Time averaged flow field (b) PSD at two selected axial locations

Fig. 5. Temporal analysis of the flow field and identification of the precessing frequency.

number, based on the mean velocity and hydraulic diameter of the jet, of $St \approx 0.13$. In the literature, the PVC has always been seen as a structure present in the flow field next to vortex breakdown as they often occur simultaneously. However, Figure 4 clearly shows that the PVC is actually the spiral mode of breakdown. This connection has not been made until now, at least not for annular jet flow. These results might be very important in the further investigation of the link between vortex breakdown and the PVC.

4. Conclusions

In this study, the instantaneous and time-averaged flow structures of an annular swirling jet flow have been studied using time-resolved tomographic particle image velocimetry measurements. Two distinct flow structures were identified. The first one is a toroidal central recirculation zone behind the centerbody. This torus is created by a swirl induced radial pressure gradient to balance the centrifugal forces. Further downstream, the conservation of tangential momentum creates

regions of high tangential velocities. This promotes vortex breakdown, which is the second large scale flow structure in the flow field. The visualization of the instantaneous flow reveals that the central vortex core breaks up into a double helix, which is wrapped around the breakdown bubble. The occurrence of this double helix mode of vortex breakdown is very rare and all studies in literature report it only in laminar swirling flows. This study is the first one to show that the vortex core already breaks up upstream of the vortex breakdown bubble and that it precesses around the central axis. This suggests that the well-known precessing vortex core observed in swirling flows is actually the spiral mode of vortex breakdown. To the authors' knowledge, this study is the first one to make the connection between these two flow features found in swirling jets.

Acknowledgements

The authors would like to thank the Flemish Fund for Scientific Research FWO-Vlaanderen and the J.M. Burgerscentrum for their financial support of the measurement campaign.

References

Alekseenko S V, Bilsky A V, Dulin V M, Markovich D M (2007) Experimental study of an impinging jet with different swirl rates. Int J of Heat and Fluid Flow 28(6):1340-1359.

Elsinga G E, Scarano F, Wieneke B, van Oudheusden, B W (2006) Tomographic particle image velocimetry. Exp Fluids 41(6):933-947.

Gupta A K, Lilley D G, Syred N (1986) Swirl flows. Abacus Press, Tunbridge Wells, England.

Jeong J, Hussain, F (1995) On the identification of a vortex. J Fluid Mech 285:69-94.

Lucca-Negro O, O'Doherty T (2001) Vortex breakdown: a review. Prog Energ Combust 27(4):431-481.

Percin M, van Oudheusden, B W (2015) Three-dimensional flow structures and unsteady forces on pitching and surging revolving flat plates. Exp Fluids 56(2):1-19.

Ruith M R, Chen P, Meiburg E, Maxworthy T (2003) Three-dimensional vortex breakdown in swirling jets and wakes: direct numerical simulation J Fluid Mech 486:331-378.

Scarano F (2012) Tomographic PIV: principles and practice. Meas Sci Technol 24(1):012001.

Syred, N (2006) A review of oscillation mechanisms and the role of the precessing vortex core (PVC) in swirl combustion systems. Prog Energ Combust 32(2):93-161.

van Oudheusden B W (2013) PIV-based pressure measurement. Meas Sci Technol 24(3):032001.

Vanierschot M, Van den Bulck E (2008) Influence of swirl on the initial merging zone of a turbulent annular jet. Phys Fluids 20(10):105104.

Vanierschot M, Persoons T, Van den Bulck E (2009) An Eulerian time filtering technique to study large-scale transient flow phenomena. Exp Fluids 47(4-5):613-626.

Vanierschot M, van Dyck K, Sas P, Van den Bulck E (2014) Symmetry breaking and vortex precession in low-swirling annular jets. Phys Fluids 26(10):105110.

Willert C E, Gharib M (1991) Digital particle image velocimetry. Exp Fluids 10(4):181-193.